Applying automated patch-clamp to disease modeling: recapitulate phenotypes of Brugada syndrome using iPSC-CMs

Wener Li[1], Xiaojing Luo[1] Ying Ulbricht[1] and Kaomei Guan[1]*

[1] Institute of Pharmacology and Toxicology, Technische Universität Dresden, Fetscherstr. 74, 01307 Dresden, Germany

* Corresponding author:

Prof. Dr. Kaomei Guan

Institute of Pharmacology and Toxicology

Technische Universität Dresden

Fetscherstr. 74

01307 Dresden, Germany

Tel: (+49)3514586246

Fax: (+49)3514586315

E-mail: kaomei.guan@tu-dresden.de

Summary

Recently, there have been great advances in cardiovascular channelopathy modeling and drug safety pharmacology using human induced pluripotent stem cell-derived cardiomyocytes (iPSC-CMs). The automated patch-clamp (APC) technique overcomes the disadvantages of manual patch-clamp (MPC) such as labor intensive and low output. However, it was not clear whether the data generated by using the APC could be reliably used for iPSC-CM disease modeling. In this study, we improved the iPSC-CM preparation method by applying 2.5 μM blebbistatin (BB, an excitation-contraction coupling uncoupler) in the whole APC procedures (dissociation, filtration, storage, and recording). Under non-BB buffered condition, iPSC-CMs in suspension showed a severe bleb-like morphology, however, BB-supplement leads to significant improvements in morphology and I_{Na} recording. We observe no effects of BB on action potential and field potential. Furthermore, APC faithfully recapitulates the single-cell electrophysiological phenotypes of iPSC-CMs derived from Brugada syndrome patients, as detected with MPC. Our study indicates that APC is capable of replacing MPC in the modeling of cardiac channelopathies using human iPSC-CMs by providing high quality data with higher throughput.

Keywords

automated patch-clamp, iPSC-derived cardiomyocytes, blebbistatin, calcium paradox, Brugada syndrome, sodium current, transient outward potassium current

Introduction

Since the development of patch-clamp techniques for high-resolution current recording from cells and cell-free membrane patches, the manual patch-clamp (MPC) technology revolutionized electrophysiological studies (Milligan et al., 2009). Despite the 'golden standard' data qualities, which are highly appreciated, the low data output is the instinctive character of MPC (Dunlop et al., 2008). So far, the modelling of cardiac channelopathies using human induced pluripotent stem cell-derived cardiomyocytes (iPSC-CMs) is mostly achieved by studying ion channels using MPC. For example, MPC was widely used in recordings of I_{Na} (voltage-gated sodium current, caused by SCN5A mutation (Liang et al., 2016) and SCN10A (El-Battrawy et al., 2019)), I_{CaL} (L-type voltage-gated calcium current, caused by CACNA1C mutation (Estes et al., 2019)), or *Ikr* (caused by KCNH2 mutation (Itzhaki et al., 2011; Shinnawi et al., 2019)) in iPSC-CMs to study cardiac channelopathies. Furthermore, the labor-intensive and low-throughput nature of MPC has hindered its large implementation in drug discovery. With these advantages and limitations in mind, the automated patch-clamp (APC) might play a key role in ion channel research as well as in drug discovery and safety testing (Stoelzle et al., 2011). However, APC poses often underestimated challenges to the reproducibility with the cells used (Dunlop et al., 2008).

The most challenging step for APC is the acquisition of a large number of single suspension iPSC-CMs in relaxation stage (Li et al., 2019). It is assumed that the Ca^{2+}-free period is necessary to allow cell separation via disruption of the Ca^{2+}-dependent cadherins (Voigt et al., 2015). However, after only a few minutes of Ca^{2+}-free perfusion and Ca^{2+} repletion, the profound changes to the cardiomyocytes, including ultrastructural alterations, loss of intracellular components, and Na^{+} and Ca^{2+} gain, were reported (Daly et al., 1987). This phenomenon was first reported as the calcium paradox (Zimmerman and Hulsmann, 1966). To conquer this paradox, excitation-contraction uncoupling agents like 2,3-butanedione monoxime (BDM) or blebbistatin (BB) were used (Voigt

et al., 2015). Nevertheless, the BDM was reported to have side effects such as reducing *Ito* (Coulombe et al., 1990), attenuating β-adrenergic response of I_{CaL} (Julio et al., 2016), and even inhibiting mitochondrial respiration (Hall and Hausenloy, 2016). On the other hand, BB was rarely reported to have electrophysiological side effects in rodents (Dou et al., 2007; Fedorov et al., 2007), but significant effects in the isolated rabbit heart (Brack et al., 2013).

In this study, we improved our previously published cell dissociation method suitable for APC (Li et al., 2019) by supplementing 2.5 μM BB in the papain-EDTA-based dissociation solution. Additionally, 2.5 μM BB was also used for strainer filtration and storage of iPSC-CMs. The extracellular solutions in the liquid handling part of APC were also supplemented with 2.5 μM BB. The protection of fragile iPSC-CMs in suspension by applying BB was beneficial to electrophysiological studies of ion channels by using APC. Our data demonstrate that BB (2.5 μM) does not exhibit any effects on action potential (AP) and field potential (FP) using human iPSC-CMs. Furthermore, we conducted ion channel studies in iPSC-CMs from patients with Brugada syndrome (BrS) by using APC. The data on I_{Na} and I_{to} were consistent with our previous data obtained by using MPC. Our study indicates that APC is capable of replacing MPC in the modeling of cardiac channelopathies using human iPSC-CMs by providing high quality data with higher throughput.

Results and discussion

Blebbistatin prevents freshly isolated iPSC-CMs from hypercontraction

In the previous study, we reported a method for iPSC-CM dissociation into a single CM suspension (Li et al., 2019). We can obtain a large quantity of flake- and rod-like relaxation CMs and store the cells at the relaxation stage for at least 2 hours, which is required for patch-clamp experiments (Figure 1A). However, we observed the calcium paradox when we switch the solution from 1.1 mM EDTA-buffered RPMI/B27 medium to the physiological external solution (containing 2 mM $CaCl_2$), which is used for APC. Almost all CMs immediately developed severe membrane blebs, no matter whether they were stored for 2 hours or only 5 minutes (Figure 1B).

Ca^{2+}-free period (1.1 mM EDTA-buffered RPMI/B27 medium) is necessary for CM separation by the disruption of the Ca^{2+}-dependent cell-cell adhesion mediated by cadherins. However, previous study showed that switching from Ca^{2+}-free to Ca^{2+}-repletion condition used for CMs led to ultrastructural alterations, loss of intracellular components, and Na^+ and Ca^{2+} gain (Daly et al., 1987). To solve this calcium paradox issue, we tested the excitation-contraction uncoupler blebbistatin (BB, 2.5 μM, myosin II inhibitor (Straight et al., 2003)) in the whole APC procedures including the dissociation, filtration, storage, and recording steps (Figure 1C). Since BB is light sensitive (Kolega, 2004), we avoid light exposure during the whole procedure. We found the iPSC-CMs in suspension maintained the relaxation state even 2 hours after dissociation when the BB-buffered RPMI/B27 medium containing 0.4 mM Ca^{2+} was used as the storage solution (Figure 1D). To meet the needs of the APC process, where 2 mM Ca^{2+}-containing physiological external solution was used for CM capturing, we switched from BB-buffered RPMI/B27 medium to BB-buffered external solution containing 2 mM $CaCl_2$. We found that the majority of CMs remained the flake- and rod-like relaxation shapes for all 4 time points (5 min, 30 min, 1 h, and 2 hours)

after approximately 1-minute of solution exchange (Figure 1E). To further test whether the flake- and rod-like shapes could persist throughout the patch progress, generally about 10 minutes, we recorded the CM morphologies and confirmed the flake-and rod-like shapes were maintained for at least 10 minutes in BB-buffered physiological external solution (Figure 1F). Our data demonstrate that BB can be used for preparation of single cell suspension and storage of human iPSC-CMs. This is consistent with previous studies showing that BB can be used for the isolation and culture of high quality and viable adult mouse CMs (Hall and Hausenloy, 2016; Kabaeva et al., 2008).

Blebbistatin shows no effects on electrical signals of iPSC-CMs

Since the electrophysiological effects of BB have been controversially reported in different species, we assessed BB effects on contractility, FP, and AP in human iPSC-CMs. By utilizing the Maestro Edge multiwell microelectrode array (MEA) and impedance system, we could record the FP and impedance-based contractility in the same culture of iPSC-CMs before and after BB treatment for 10 min (Figure 2A-C). The contractility was abolished in most iPSC-CM cultures after the application of 2.5 μM BB for 3-5 minutes (Figure 2A, B), which is mainly due to the binding of BB to myosin II. However, the FP metrics such as spontaneous excitation frequency (Hz), spike amplitude (mV), and conduction velocity (cm/s) did not alter (Figure 2B and C). These data indicate that the BB treatment has no effects on electrical field potential of human iPSC-CMs but prevents their beating. Our study is consistent with previous studies, in which the treatments with 1 μM (Guo et al., 2011) and 10 μM (Qian et al., 2017) BB did not show any effects on FP of human iPSC-CMs. Moreover, with the prolonged incubation of human iPSC-CMs with 2.5 μM BB till 1 hour, we did not observe differences in FP parameters (Supplementary Figure 1).

We then investigated the effects of 2.5 µM BB treatment on AP morphologies of iPSC-CMs by using MPC when the cells were paced at 0.5 Hz. We did not observe any differences in AP duration at 90% repolarization (APD90), AP amplitude (APA), and resting membrane potential (RMP) before and after the treatment with 2.5 µM BB for 10 min (Figure 2D and E). Similar results showing no effect of treatment with 10 µM BB for 5 min on AP duration were reported in isolated mouse CMs (Dou et al., 2007). Furthermore, superfusion of an explanted zebrafish embryonic heart with BB (1, 5 and 10 µM) was reported to have no effects on AP morphology and AP parameters including APD, RMP and maximum upstroke velocity in both atrial and ventricular CMs (Jou et al., 2010). Superfusion with 10 µM BB for 60 min also did not induce any changes in AP morphologies paced at 2.5 Hz as registered by microelectrodes from preparations of rabbit atria and ventricles (Fedorov et al., 2007). However, another study showed that the 60-min perfusion with BB (5 µM) significantly prolonged optically recorded APs and corrected QT interval on ECG (Brack et al., 2013).

Blebbistatin does not alter the magnitude of intracellular calcium transient

To study whether 2.5 µM BB application affects intracellular calcium transient, human iPSC-CMs were labelled with the ratio-metric fluorescent calcium indicator Fura-2 (Figure 2F, G). Our data showed that BB has no effect on Ca^{2+} transient morphology as well as parameters such as amplitude, systolic Ca^{2+} level (Figure 2F, G), or decay rate (before: 1.03 ± 0.015; after: 1.04 ± 0.014; $p = 0.576$). After 5 min, 2.5 µM BB application led to the reduction of diastolic Ca^{2+} level from 0.76 ± 0.009 to 0.71 ± 0.009 ($n = 18$ from 4 differentiations, paired, $p < 0.001$) in iPSC-CMs paced at 0.25 Hz. Similar results were observed in rat cardiomyocytes loaded with the ratio-metric fluorescent calcium indicator Indo-1 (Farman et al., 2008). Whereas Ca^{2+} transient amplitude, and

the decay were not affected by 1 h application of 0.5 μM Blebbistatin, diastolic Ca^{2+} level revealed a slight reduction after BB application (Farman et al., 2008). Notably, BB application resulted in significant elevations of diastolic fluorescence level in rat cardiomyocytes labelled with the non-ratiometric fluorescent calcium indicator Fluo-4 (Farman et al., 2008) or labelled with another non-ratiometric indicator Fluo-5F (Fedorov et al., 2007) whereas BB did not affect the intracellular Ca^{2+} transient amplitude as assessed by either Fluo-4 or Fluo-5F. Since both Fluo-4 and Fluo-5F are not ratio-metric, therefore, the increase in diastolic fluorescence must be interpreted with caution. Given differences observed by applications of different ratio-metric or non-ratiometric fluorescent indicators, we can speculate that light-sensitive BB tangles with different dyes.

Blebbistatin maintains the function of sodium channels

To evaluate whether the relaxation morphologies and state of iPSC-CMs achieved by BB supplement during the whole experimental process (dissociation, straining, storage, and APC recording) make significant differences for current recording, we first recorded I_{Na} by using physiological external solution containing 140 mM $[Na^+]_o$ (Figure 3A). Unlike the control group without BB, in the group with 2.5 μM BB supplement, the majority of I_{Na} activation stages lost voltage control (Figure 3A), a sign of too high extracellular Na^+ concentration for patch-clamp. We even have four 'out-of-gain' recordings using the APC gain setting (0.5 mV/pA for a maximum of 20 nA). In the control group without BB, the peak I_{Na} (-183.4 ± 22.5 pA/pF) appeared at -15 mV while in the group with BB, the peak I_{Na} of -307.2 ± 35.1 pA/pF (n = 51) was found at -25 mV (Figure 3B). These results suggest that BB supplement make a significant improvement for I_{Na} recording.

To prevent the loss of voltage control during I_{Na} recording, we reduced the extracellular Na^+ concentration to 50 mM (Figure 4A, B). Under this condition, none of the iPSC-CMs in the group with BB showed the 'out-of-gain' I_{Na}. To this end, we repeated I_{Na} recording using APC in previously published BrS disease models (Li et al., 2020). In the presence of 2.5 μM BB, single iPSC-CMs were obtained from two healthy donors (Ctrl1 and Ctrl2) and two BrS patients (BrS1 and BrS2, harboring the same *SCN5A* p.S1812X mutation. As shown in Figure 4A, the I_{Na} density in BrS-CMs was dramatically lower compared to that in Ctrl-CMs. Under the testing potentials ranging from -40 mV to 15 mV, I_{Na} densities in both BrS1- and BrS2-CMs were significantly smaller than in Ctrl1- and Ctrl2-CMs (Figure 4B). The peak I_{Na} appeared at -20 mV in Ctrl1- and Ctrl2-CMs showed as -114.9 ± 11.7 and -117.5 ± 20.7 pA/pF, and in BrS1- and BrS2-CMs presented as -63.5 ± 7.3 and -45.9 ± 6.0 pA/pF, respectively. These results generated by using APC were consistent with our previous results acquired using MPC, which also revealed a more than 50% reduction of I_{Na} density in BrS-CMs (Li et al., 2020).

Blebbistatin has no effect on I_{to} and I_{CaL} recording

The peak I_{to} at +60 mV in BrS1-CMs (9.7 ± 2 pA/pF) and BrS2-CMs (10.8 ± 2.2 pA/pF) were significantly bigger than those in Ctrl1-CMs (4.7 ± 0.5 pA/pF) and Ctrl2-CMs (5.7 ± 0.8 pA/pF) (Figure 4C and D). The I_{to} recorded with APC are in line with our previous publication of MPC results: the I_{to} at +60 mV in BrS1-CMs and BrS2-CMs were 2.4 and 1.9 times bigger than those in Ctrl-CMs (Li et al., 2020). Furthermore, consistent with our MPC data, we did not observe any I_{CaL} density differences between Ctrl-CMs and BrS-CMs (Figure 4 E, F).

Taken together, we firstly improve iPSC-CM preparation for APC recording in this study. By supplement of BB to the whole procedures (dissociation, filtration, storage, and recording), we can make significant promotions not only in obtaining relax iPSC-CMs but also in I_{Na} recording. Furthermore, APC faithfully recapitulates the single-cell electrophysiological phenotypes of iPSC-CMs derived from BrS patients, as detected with MPC. Our study suggests APC is capable of replacing MPC in the modeling of cardiac channelopathies using human iPSC-CMs by providing high quality data with higher throughput.

Experimental procedures

Directed differentiation of iPSCs into iPSC-CMs

Directed differentiation of iPSCs into ventricular-like CMs was induced by modulating WNT signaling as previously described (Cyganek et al., 2018). When iPSCs (cultured on 12-well plates) reached around 90% confluency, differentiation was initiated by changing medium into cardio differentiation medium (RPMI 1640 with GlutaMax and HEPES (Thermo Fisher Scientific), 0.5 mg/ml human recombinant albumin (Sigma-Aldrich) and 0.2 mg/ml L-ascorbic acid 2-phosphate (Sigma-Aldrich)) supplemented with 4 µM of the GSK3β inhibitor CHIR99021 (Millipore). After 48 hours, the medium was changed to fresh cardio differentiation medium supplemented with 5 µM IWP2 (WNT signaling inhibitor, Millipore) for another two days. Afterward, cells were cultured in the cardio differentiation medium for another 4 days. From day eight on, the cardiac differentiation medium was replaced by RPMI/B27 medium (RPMI 1640 with GlutaMax and HEPES, supplemented with 2% B27 with insulin (Thermo Fisher Scientific)). On day 20, beating cardiomyocytes were detached from plates with 1 mg/ml collagenase B (Worthington Biochemical), dissociated with 0.25% Trypsin/EDTA (Thermo Fisher Scientific), and replated into Geltrex-coated 6-well plates at a density of 800,000 cells/well. Afterward, iPSC-CMs were cultured in RPMI/B27 medium for around 3 months.

Dissociation of 3-month-old iPSC-CMs into single cells for automated patch-clamp

Our previously published dissociation method was used in this study with some modifications (Li et al., 2019). Collagenase B (1 mg/ml) was used to pre-treat 3-month-old iPSC-CMs until the layer of cardiomyocytes detached. The layer of cardiomyocytes was transferred into a 3.5-cm dish and then treated with 2 ml of 20 U/ml papain (Sigma-Aldrich) dissolved in 1.1 mM EDTA buffered

RPMI/B27 medium containing 2.5 µM BB (Sigma-Aldrich, dissolved in DMSO as 10 mM stock) for 10 min. A fire-polished glass Pasteur pipette was used to gently agitate the cells to release single iPSC-CMs. The cell suspension was filtered through a 30-µm strainer (MACS SmartStrainers, Miltenyi Biotec) to remove cell clusters and was centrifuged for 1 min at 50 g. After gently aspirating the supernatant, the cell pellet was resuspended into 2 ml of 1.1 mM EDTA buffered RPMI/B27 medium (+2.5 µM BB) and then filtered through a 10-µm strainer (pluriStrainer®, pluriSelect) to collect larger iPSC-CMs. The cells were collected with 2 ml of RPMI/B27 medium with 2.5 µM BB and then centrifuged for 1 min at 50 g. After removing the supernatant, the cell pellet was gently aspirated and further stored in 2.5 µM BB containing RPMI/B27 medium at 4 °C for 2 h.

Contractility and FP measurements

For the measurements of contractility and FP together in the same culture, the Maestro Edge multiwell microelectrode array (MEA) and impedance system (Axion BioSystems) was used. The 3-month-old iPSC-CMs were seeded into Cytoview MEA 6-well or 24-well plate (Axion BioSystems) according to the protocol provided by Axion BioSystems. Every well was coated with Geltrex® (Thermo Fisher Scientific) for at least 1 hour. The 0.25% Trypsin-EDTA dissociated cells were seeded as density 10,000/8 µl to one well of the plate. The medium was changed one day after plating and thereafter every two days until day 6. On day 6, electrical FP and the impedance-based contractility in human iPSC-CMs were measured before and after 2.5 µM BB treatment. After calibrating for 10 minutes, the spontaneous recordings were carried out at 37 °C and 5% CO_2 using AxIS Navigator software (Axion BioSystems). The sample rates were 12,500 Hz for FP and 40 Hz for contractility. Spontaneous beating frequency was defined by the reciprocal

of averaged inter-beat interval. The spontaneous beating frequency, FP amplitude, and conduction velocity were generated by AxIS Navigator and further analyzed by AxIS Metric Plotting Tool (Axion BioSystems). The mainstream conduction velocity values were averaged for one culture.

Manual patch-clamp for AP measurement

iPSC-CMs around day 90 were enzymatically dissociated into single cells and seeded on 5 mm Ø coverslips distributed in 35-mm dishes. After around 10 days for recovery, the paced APs of a single iPSC-CM were measured at room temperature with a ruptured whole-cell current clamp using HEKA EPC10 amplifier and Patchmaster (HEKA Elektronik). The pipette and extracellular solutions for paced APs recordings were listed in Supplementary Table 1. The pacing stimulus was 0.5 Hz. Pipette potentials were corrected for liquid junction potentials. More than 5 continuously stable paced APs were chosen and analyzed using LabChart® (ADInstruments) to determine APD90, APA, and RMP.

Calcium transient measurement

Paced whole-cell calcium transients were measured according to our previous publication (Luo et al., 2020). CMs around day 80 were dissociated and replated on coverslips at a density of 200,000 cells/well (6 well plate). Cells recovered for at least 10 days were loaded with Fura-2 (Thermo Fisher Scientific) at a final concentration of 5 μM in RPMI/B27 medium for 30 min at 37 °C and washed twice with the medium. Before measurement, cells were incubated for 10 min to enable complete de-esterification of intracellular Fura-2. Calcium transients were recorded using a 40× objective on an Olympus IX70 microscope fitted with an IonWizard software (IonOptix) at 35 °C.

Samples were excited at 340 and 380 nm with a switching frequency of 200 Hz and the emitted fluorescence was collected at 510 nm. The cytosolic Ca^{2+} level was measured as the ratio of fluorescence at 340 and 380 nm (340/380 nm) in Tyrode's solution. To minimize the phototoxicity and photoinactivation effects of BB, the recording was paused during the BB exposure time. To normalize the Ca^{2+} transient frequency, iPSC-CMs were field-stimulated using a MyoPacer (IonOptix) at a pacing frequency of 0.25 Hz (6 V, 10 ms). The monotonic transient analysis was performed using the LabChart® (ADInstruments) and the following parameters were determined: peak amplitude of Ca^{2+} transients (the Fura-2 ratio at systole subtracted by the Fura-2 ratio at diastole), decay rate (tau), as well as duration of Ca^{2+} transients.

Automated patch-clamp

All experiments were performed at room temperature using an automated patch-clamp system (Patchliner Quattro, Nanion Technologies GmbH) with low resistance NPC-16 chips. The pipette and extracellular solutions for I_{Na}, *Ito*, and I_{CaL} recordings were listed in Supplementary Table 1. From a holding potential of -100 mV, I_{Na} was recorded using voltage steps from -80 to +70 mV for 20 ms in 5 mV steps at an interval of 2000 ms (shown as an inset in Figure 3B and 4B). Nifedipine (10 μM) was used to block I_{CaL}. *Ito* was recorded by increasing the testing potential stepwise from -40 mV to +60 mV in 10 mV steps from a holding potential of -90 mV with a 20 ms pre-pulse to -35 mV to inactivate I_{Na} (shown as an inset in Figure 4D). $CdCl_2$ (0.5 mM) was used to block calcium current. Each pulse lasted for 400 ms, the sweep interval was 10 s. To record I_{CaL}, cells were depolarized for 100 ms to voltages between -80 to 50 mV from a holding potential of -90 mV, the sweep interval was 3 s (shown as an inset in Figure 4F). Currents were sampled at 25 kHz and low-pass-filtered at 2.9 kHz. The liquid junction potentials and series resistance were

not compensated for all recordings. The data were exported by using Patchmaster and further analyzed with Graph Pad Prism 5 (GraphPad Software, Inc).

Statistics

Statistical analysis was performed with GraphPad Prism 5 using the paired Student's *t*-test to compare differences between two paired groups, and the two-way ANOVA with Bonferroni post-test for comparison of more groups and conditions. Data are presented as the mean ± standard error of the mean (SEM). Results were considered statistically significant when the p-value was <0.05.

Author Contributions

WL and KG conceived the study and designed experiments. WL, XL, and YU performed experiments and acquired data. WL, XL, and KG analyzed and interpreted the data. WL and KG wrote the manuscript.

Acknowledgments

We thank Konstanze Fischer, Jessie Pöche, and Judith Müller for excellent technical assistance. The authors would like to express great appreciation to Free State of Saxony and the European Union EFRE (SAB project "PhänoKard" and "PhenoCor" to K.G.).

References

Brack, K.E., Narang, R., Winter, J., and Ng, G.A. (2013). The mechanical uncoupler blebbistatin is associated with significant electrophysiological effects in the isolated rabbit heart. Exp Physiol *98*, 1009-1027.

Coulombe, A., Lefevre, I.A., Deroubaix, E., Thuringer, D., and Coraboeuf, E. (1990). Effect of 2,3-butanedione 2-monoxime on slow inward and transient outward currents in rat ventricular myocytes. Journal of molecular and cellular cardiology *22*, 921-932.

Cyganek, L., Tiburcy, M., Sekeres, K., Gerstenberg, K., Bohnenberger, H., Lenz, C., Henze, S., Stauske, M., Salinas, G., Zimmermann, W.H., et al. (2018). Deep phenotyping of human induced pluripotent stem cell-derived atrial and ventricular cardiomyocytes. JCI Insight *3*.

Daly, M.J., Elz, J.S., and Nayler, W.G. (1987). Contracture and the calcium paradox in the rat heart. Circulation research *61*, 560-569.

Dou, Y., Arlock, P., and Arner, A. (2007). Blebbistatin specifically inhibits actin-myosin interaction in mouse cardiac muscle. American Journal of Physiology-Cell Physiology *293*, C1148-C1153.

Dunlop, J., Bowlby, M., Peri, R., Vasilyev, D., and Arias, R. (2008). High-throughput electrophysiology: an emerging paradigm for ion-channel screening and physiology. Nat Rev Drug Discov *7*, 358-368.

El-Battrawy, I., Albers, S., Cyganek, L., Zhao, Z., Lan, H., Li, X., Xu, Q., Kleinsorge, M., Huang, M., Liao, Z., et al. (2019). A cellular model of Brugada syndrome with SCN10A variants using human-induced pluripotent stem cell-derived cardiomyocytes. Europace.

Estes, S.I., Ye, D., Zhou, W., Dotzler, S.M., Tester, D.J., Bos, J.M., Kim, C.S.J., and Ackerman, M.J. (2019). Characterization of the CACNA1C-R518C Missense Mutation in the Pathobiology of Long-QT Syndrome Using Human Induced Pluripotent Stem Cell Cardiomyocytes Shows Action Potential Prolongation and L-Type Calcium Channel Perturbation. Circ Genom Precis Med *12*, e002534.

Farman, G.P., Tachampa, K., Mateja, R., Cazorla, O., Lacampagne, A., and de Tombe, P.P. (2008). Blebbistatin: use as inhibitor of muscle contraction. Pflugers Arch *455*, 995-1005.

Fedorov, V.V., Lozinsky, I.T., Sosunov, E.A., Anyukhovsky, E.P., Rosen, M.R., Balke, C.W., and Efimov, I.R. (2007). Application of blebbistatin as an excitation-contraction uncoupler for electrophysiologic study of rat and rabbit hearts. Heart rhythm : the official journal of the Heart Rhythm Society *4*, 619-626.

Guo, L., Abrams, R.M., Babiarz, J.E., Cohen, J.D., Kameoka, S., Sanders, M.J., Chiao, E., and Kolaja, K.L. (2011). Estimating the risk of drug-induced proarrhythmia using human induced pluripotent stem cell-derived cardiomyocytes. Toxicol Sci *123*, 281-289.

Hall, A.R., and Hausenloy, D.J. (2016). Mitochondrial respiratory inhibition by 2,3-butanedione monoxime (BDM): implications for culturing isolated mouse ventricular cardiomyocytes. Physiological reports *4*, e12606.

Itzhaki, I., Maizels, L., Huber, I., Zwi-Dantsis, L., Caspi, O., Winterstern, A., Feldman, O., Gepstein, A., Arbel, G., Hammerman, H., et al. (2011). Modelling the long QT syndrome with induced pluripotent stem cells. Nature *471*, 225-229.

Jou, C.J., Spitzer, K.W., and Tristani-Firouzi, M. (2010). Blebbistatin effectively uncouples the excitation-contraction process in zebrafish embryonic heart. Cellular physiology and biochemistry : international journal of experimental cellular physiology, biochemistry, and pharmacology *25*, 419-424.

356 Julio, A.-C., Ana Iris, L.-M., Loipa, G.-M., and Julio, L.A. (2016). 2,3-Butanedione monoxime
357 attenuates the β-adrenergic response of the L-type Ca2+ current in rat ventricular
358 cardiomyocytes. Journal of Pharmacy & Pharmacognosy Research *4*, 206-216.
359 Kabaeva, Z., Zhao, M., and Michele, D.E. (2008). Blebbistatin extends culture life of adult
360 mouse cardiac myocytes and allows efficient and stable transgene expression. Am J Physiol
361 Heart Circ Physiol *294*, H1667-1674.
362 Kolega, J. (2004). Phototoxicity and photoinactivation of blebbistatin in UV and visible light.
363 Biochem Biophys Res Commun *320*, 1020-1025.
364 Li, W., Luo, X., Ulbricht, Y., Wagner, M., Piorkowski, C., El-Armouche, A., and Guan, K.
365 (2019). Establishment of an automated patch-clamp platform for electrophysiological and
366 pharmacological evaluation of hiPSC-CMs. Stem cell research *41*, 101662.
367 Li, W., Stauske, M., Luo, X., Wagner, S., Vollrath, M., Mehnert, C.S., Schubert, M., Cyganek,
368 L., Chen, S., Hasheminasab, S.M., et al. (2020). Disease Phenotypes and Mechanisms of iPSC-
369 Derived Cardiomyocytes From Brugada Syndrome Patients With a Loss-of-Function SCN5A
370 Mutation. Front Cell Dev Biol *8*, 592893.
371 Liang, P., Sallam, K., Wu, H., Li, Y., Itzhaki, I., Garg, P., Zhang, Y., Vermglinchan, V., Lan, F.,
372 Gu, M., et al. (2016). Patient-Specific and Genome-Edited Induced Pluripotent Stem Cell-
373 Derived Cardiomyocytes Elucidate Single-Cell Phenotype of Brugada Syndrome. Journal of the
374 American College of Cardiology *68*, 2086-2096.
375 Luo, X., Li, W., Kunzel, K., Henze, S., Cyganek, L., Strano, A., Poetsch, M.S., Schubert, M.,
376 and Guan, K. (2020). IP3R-Mediated Compensatory Mechanism for Calcium Handling in
377 Human Induced Pluripotent Stem Cell-Derived Cardiomyocytes With Cardiac Ryanodine
378 Receptor Deficiency. Front Cell Dev Biol *8*, 772.
379 Milligan, C.J., Li, J., Sukumar, P., Majeed, Y., Dallas, M.L., English, A., Emery, P., Porter, K.E.,
380 Smith, A.M., McFadzean, I., et al. (2009). Robotic multiwell planar patch-clamp for native and
381 primary mammalian cells. Nature protocols *4*, 244-255.
382 Qian, F., Huang, C., Lin, Y.D., Ivanovskaya, A.N., O'Hara, T.J., Booth, R.H., Creek, C.J.,
383 Enright, H.A., Soscia, D.A., Belle, A.M., et al. (2017). Simultaneous electrical recording of
384 cardiac electrophysiology and contraction on chip. Lab on a chip *17*, 1732-1739.
385 Shinnawi, R., Shaheen, N., Huber, I., Shiti, A., Arbel, G., Gepstein, A., Ballan, N., Setter, N.,
386 Tijsen, A.J., Borggrefe, M., et al. (2019). Modeling Reentry in the Short QT Syndrome With
387 Human-Induced Pluripotent Stem Cell–Derived Cardiac Cell Sheets. Journal of the American
388 College of Cardiology *73*, 2310-2324.
389 Stoelzle, S., Obergrussberger, A., Bruggemann, A., Haarmann, C., George, M., Kettenhofen, R.,
390 and Fertig, N. (2011). State-of-the-Art Automated Patch Clamp Devices: Heat Activation,
391 Action Potentials, and High Throughput in Ion Channel Screening. Front Pharmacol *2*, 76.
392 Straight, A.F., Cheung, A., Limouze, J., Chen, I., Westwood, N.J., Sellers, J.R., and Mitchison,
393 T.J. (2003). Dissecting temporal and spatial control of cytokinesis with a myosin II Inhibitor.
394 Science *299*, 1743-1747.
395 Voigt, N., Pearman, C.M., Dobrev, D., and Dibb, K.M. (2015). Methods for isolating atrial cells
396 from large mammals and humans. Journal of molecular and cellular cardiology *86*, 187-198.
397 Zimmerman, A.N., and Hulsmann, W.C. (1966). Paradoxical influence of calcium ions on the
398 permeability of the cell membranes of the isolated rat heart. Nature *211*, 646-647.

399

400 **Figure Titles and Legends**

Figure 1

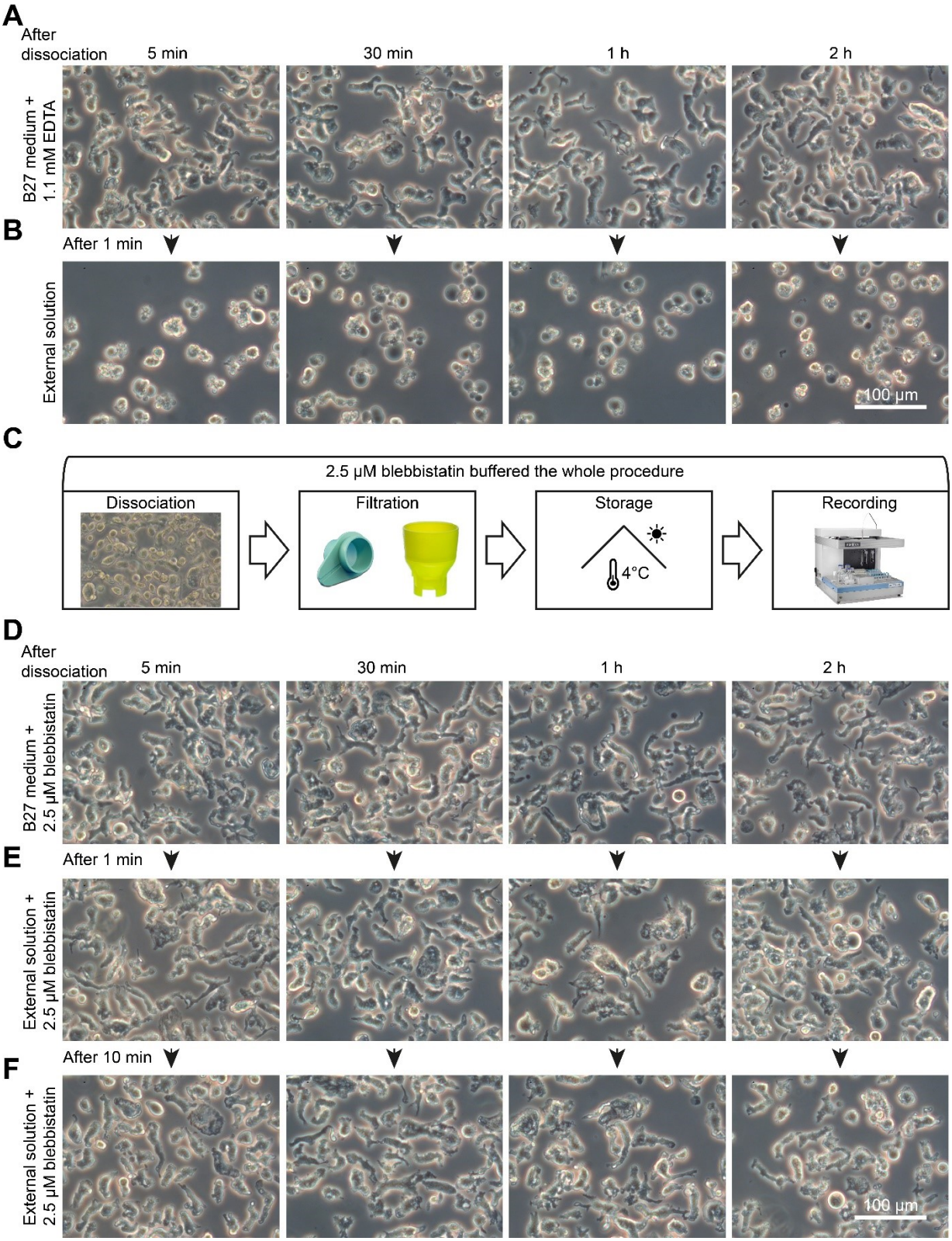

401

Figure 1. Morphological observations of dissociated iPSC-CMs in suspension under different conditions. (**A**) The morphologies of iPSC-CMs in suspension in 1.1 mM EDTA-buffered RPMI/B27 medium for 5 min, 30 min, 1 hour, and 2 hours. (**B**) The morphological changes after the CMs are transferred from EDTA-buffered RPMI/B27 medium to 2 mM Ca^{2+}-containing physiological external solution, corresponding to the 4 different time points. (**C**) For the improved iPSC-CM preparation method, 2.5 μM BB was used to buffer the whole procedure including cell dissociation, filtration, storage, and recording. (**D**) The morphologies of iPSC-CMs in 2.5 μM BB-buffered RPMI/B27 medium for 5 min, 30 min, 1 hour, and 2 hours. (**E-F**) Correspondingly to different time points, shown are morphologies after the identical CMs transferred from BB-buffered RPMI/B27 medium to BB-buffered, 2 mM Ca^{2+}-containing physiological external solution for 1 min (**E**) and 10 min (**F**). Scale bar: 100 μm.

Figure 2

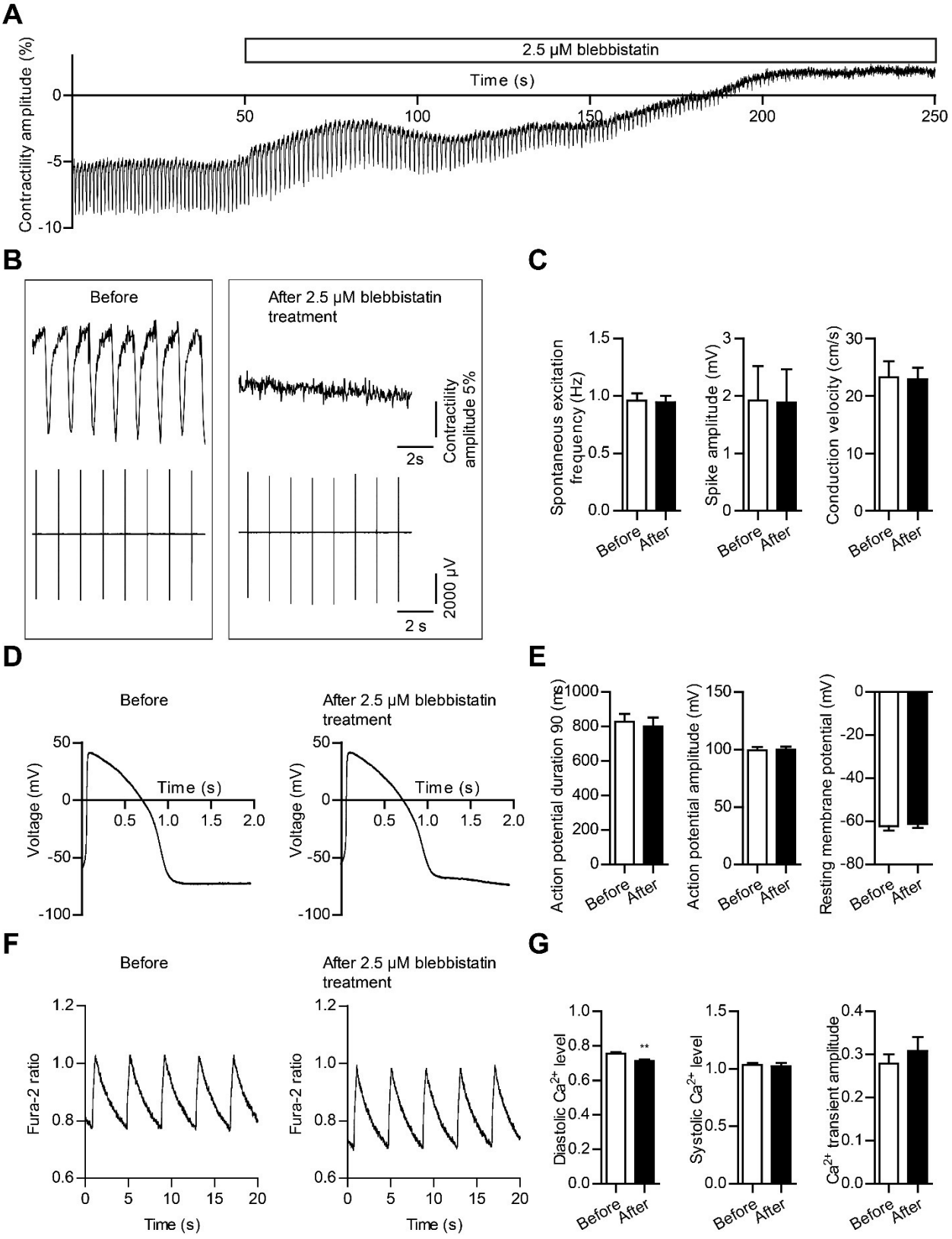

416

417 **Figure 2. Blebbistatin uncouples the excitation and contraction of iPSC-CMs.** (**A**) The
418 representative contractility trace demonstrated the iPSC-CM monolayer culture stopped beating
419 3–5 minutes after 2.5 μM BB treatment. (**B**) Original contractility and FP traces in the same iPSC-
420 CM culture before and after 2.5 μM BB treatment. (**C**) Statistical analyses of FP metrics:
421 spontaneous excitation frequency (**left**), spike amplitude (**middle**), and conduction velocity (**right**).
422 n = 14 cultures from 5 differentiation experiments for spontaneous excitation frequency and spike
423 amplitude. n = 7 cultures from 3 differentiation experiments for conduction velocity. (**D**)
424 Representative 0.5 Hz paced AP before and after 2.5 μM BB treatment for 10 minutes. (**E**)
425 Statistical analyses of AP metrics: AP duration 90 (**left**), AP amplitude (**middle**), and resting
426 membrane potential (**right**). n = 11 cells from 5 differentiation experiments for all the three AP
427 parameters. (**F**) Representative 0.25 Hz paced calcium transients before and after 2.5 μM BB 5
428 min treatment. (**G**) Statistical analyses of calcium transients metrics: diastolic Ca^{2+} level (**left**), and
429 systolic Ca^{2+} level (**middle**) and Ca^{2+} transients amplitude (**right**). n = 18 from 4 differentiation
430 experiments for all the three calcium transients parameters. Data are represented as mean ± SEM.
431 $p < 0.05$ was considered as significant under the paired Student's *t*-test (**$p < 0.001$).

432

Figure 3

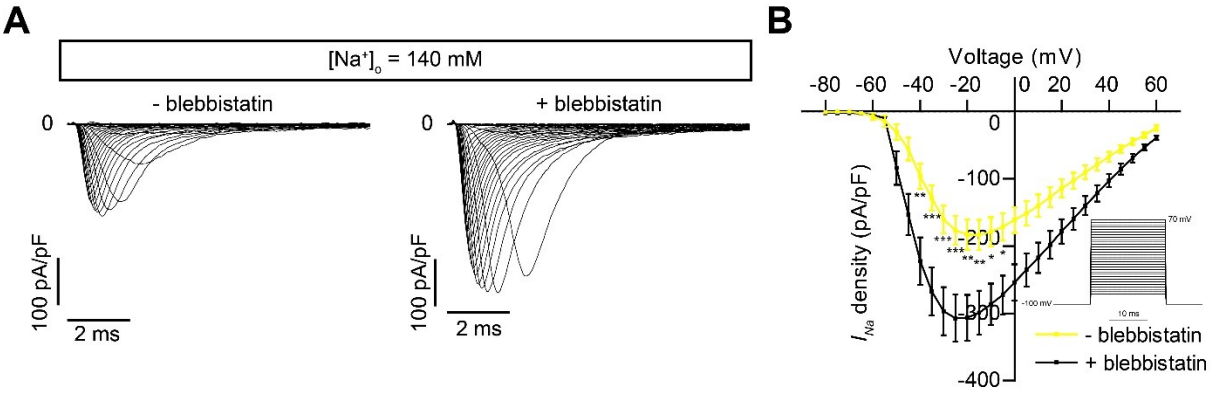

433

Figure 3. I_{Na} (under 140 mM $[Na^+]_o$) recording with/without BB buffering. (**A**) The representative I_{Na} traces in 140 mM $[Na^+]_o$ buffered with 2.5 μM BB in the whole procedures (including dissociation, filtration, storage, and recording), or without BB. (**B**) Statistical analysis of I_{Na} in 140 mM $[Na^+]_o$ (± blebbistatin buffered whole procedure). -blebbistatin: n = 29 cells from 6 differentiation experiments; +blebbistatin: n = 51 cells from 9 differentiation experiments. The stimulation protocol is shown as an inset. The stimulation protocol is shown as an inset. Data are represented as mean ± SEM. *p <0.05; **p <0.01; ***p <0.001 by two-way ANOVA with Bonferroni post-test.

Figure 4

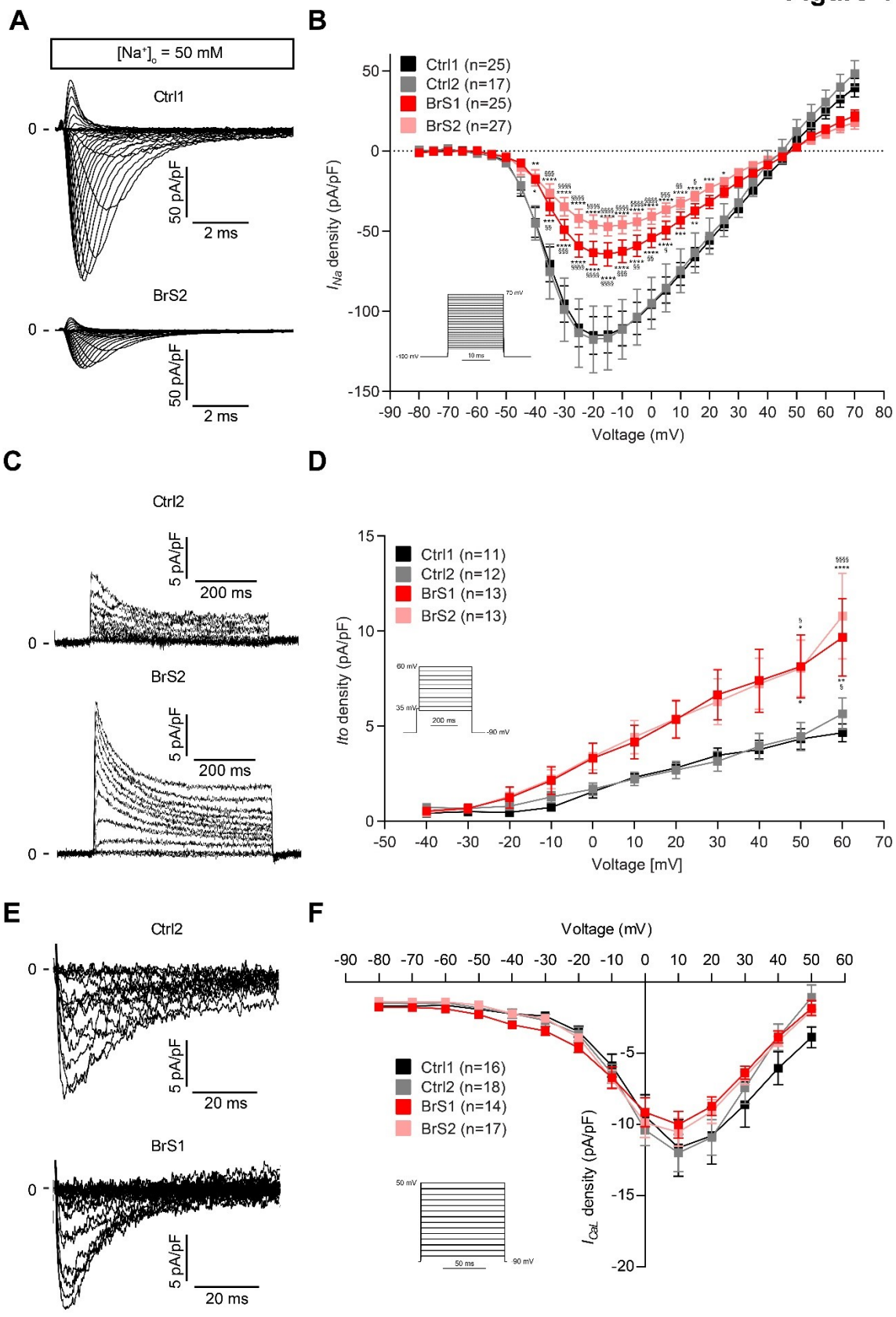

442

Figure 4. I_{Na} (under 50 mM $[Na^+]_o$), *Ito* and I_{CaL} recording for Ctrl- and BrS-CMs buffered with 2.5 µM BB in the whole procedure. (**A**) Shown are I_{Na} recordings (under 50 mM $[Na^+]_o$) in Ctrl1- and BrS2-CMs. (**B**) The *I-V* curve of I_{Na} for Ctrl1-, Ctrl2-, BrS1- and BrS2-CMs. Ctrl1: n = 25 cells from 4 differentiation experiments; Ctrl2: n = 17 cells from 3 differentiations; BrS1: n = 25 cells from 7 differentiations; BrS2: n = 27 cells from 7 differentiations. (**C**) Representative traces of *Ito* in Ctrl2- and BrS2-CMs. (**D**) *Ito* density plot in Ctrl1-, Ctrl2-, BrS1, and BrS2-CMs. Ctrl1: n = 11 cells from 4 differentiations; Ctrl2: n = 12 cells from 6 differentiations; BrS1: n = 13 cells from 6 differentiations; BrS2: n = 13 cells from 5 differentiations. (**E**) Shown are I_{CaL} recording in Ctrl2- and BrS1-CMs. (**F**) The *I-V* curve of I_{CaL} for Ctrl1-, Ctrl2-, BrS1- and BrS2-CMs. Ctrl1: n = 16 cells from 5 differentiations; Ctrl2: n = 18 cells from 7 differentiations; BrS1: n = 14 cells from 4 differentiations; BrS2: n = 17 cells from 3 differentiations. The stimulation protocols are shown as insets. Data are represented as mean ± SEM. *p <0.05; **p <0.01; ***p <0.001; ****p <0.0001 BrS *vs.* Ctrl1 by using two-way ANOVA with Bonferroni post-test. §p <0.05; §§p <0.01; §§§p <0.001; §§§§p <0.0001 BrS *vs.* Ctrl2 by using two-way ANOVA with Bonferroni post-test.